Available online at www.sciencedirect.com

SciVerse ScienceDirect

Ceramics International 38 (2012) 2507–2512

CERAMICS INTERNATIONAL

www.elsevier.com/locate/ceramint

Preparation and characterization of tetragonal dominant nanocrystalline ZrO_2 obtained via direct precipitation

Nidhi Garg [a], Vinit K. Mittal [a], Santanu Bera [a], Arup Dasgupta [b], Velmurugan Sankaralingam [a,*]

[a] Water and Steam Chemistry Division, BARC Facilities, Kalpakkam 603 102, Tamil Nadu, India
[b] Physical Metallurgy Group, IGCAR, Kalpakkam 603 102, Tamil Nadu, India

Received 22 July 2011; received in revised form 4 November 2011; accepted 7 November 2011
Available online 15 November 2011

Abstract

Nanocrystalline ZrO_2 has been prepared by using $ZrO(NO_3)_2{\cdot}6H_2O$ through direct precipitation followed by calcination. Transmission Electron Microscopic characterization of the powder shows the particle size dominantly of the order of 10 nm. The X-ray diffraction pattern shows the formation of both tetragonal and monoclinic phases where the tetragonal phase is dominant. The estimation of tetragonal phase has been carried out using the Raman scattering spectroscopy. Zeta potential of suspended ZrO_2 in aqueous medium with surfactant has been measured at varying pH and temperature to understand the effects of temperature at the interface of nanocrystalline ZrO_2 in water.

Keywords: Nanocrystalline zirconia; Direct precipitation; Zeta potential

1. Introduction

Zirconia is an important ceramic material due to its versatile properties [1]. Recently, ZrO_2 has attracted considerable attention in corrosion science because of its possible application in preventing high temperature aqueous corrosion of stainless steel [2–4]. ZrO_2 is a wide band gap material and suitable for inhibitive protective coating of stainless steel. In principle, ZrO_2 coating stops the redox reaction occurring at grain boundaries of stainless steel in presence of dissolved oxygen which is known to aggravate inter-granular corrosion cracking.

Zirconia has three stable crystal forms: monoclinic (up to 1170 °C), tetragonal (1170–2370 °C) and cubic (2370–2680 °C) [5]. The tetragonal form can be retained in a metastable state at room temperature by adding various oxides, in particular yttria [5] or by decreasing the particle size below a certain critical size [6,7]. In case of thin films (nm range), tetragonal zirconia is more stable [8]. Tetragonal structures have higher strength and toughness compared to monoclinic zirconia. Higher toughness of tetragonal zirconia can be understood in terms of transformation toughening [9]. In thin films, zirconia particles interact around a propagating crack of the substrate at the crack tip zone and the metastable tetragonal particles in the crack tip zone transform to the monoclinic crystal structure. The tetragonal to monoclinic transformation is associated with 4% increase in volume. Due to this volume expansion, crack tip compresses which retards crack growth. This leads to enhancement of fracture toughness of coatings made with metastable tetragonal zirconia particles [10]. So, it is advantageous to produce a predominant tetragonal phase in ZrO_2 coating. Several routes are followed for forming the zirconia coating viz. pulsed laser deposition [11], chemical vapour deposition [12], plasma spraying [13], electro-deposition [14], laser engineered net shaping (LENS) [15], hydrothermal [16,17] and sol–gel [18]. Most of the physical techniques used for coating the surfaces are difficult to implement at industrial scale as well as systems having complex designs. Hence, among the other techniques, hydrothermal method is more suitable because of its simplicity and applicability for industrial scale. Also the method is suitable for systems with complex designs.

Forming ZrO_2 coating by directly depositing the ZrO_2 nano powder over stainless steel through hydrothermal process is challenging and promising [19]. In this process, the phase of the coating can be controlled. Tetragonal phase of zirconia is

* Corresponding author. Tel.: +91 4427480097; fax: +91 4427480097.
E-mail address: svelu@igcar.gov.in (V. Sankaralingam).

0272-8842/$36.00
doi:10.1016/j.ceramint.2011.11.020

preferred as compared to monoclinic phase for a stable protective coating on stainless steel. In the process of nucleation of the ZrO_2 coating, it is known that the electrostatic interaction between the substrate and the suspended particles [20] play the major role. So, it is essential to know the surface charge of ZrO_2 nano particles suspended in aqueous solution [21] for properly maintaining the experimental parameters such as pH and type of dispersants [22] in the solution. In this article, the preparation of nanocrystalline zirconia powder by precipitation [23] route has been reported. Here, efforts have been made to form dominantly tetragonal zirconia powder by producing high quality nanocrystalline ZrO_2 particles. Prepared Zirconia powder was characterized for its phase determination, size distribution and chemical composition by X-ray diffraction (XRD), Transmission Electron Microscopy (TEM) and X-ray photoelectron spectroscopy (XPS) techniques, respectively. Zeta potential of the nanocrystalline zirconia powder was studied as a function of pH at various temperatures and with the addition of surfactant.

2. Experimental details

2.1. Materials synthesis

Nanocrystalline ZrO_2 was prepared through direct precipitation process by using $ZrO(NO_3)_2{\cdot}6H_2O$ (Fluka), $NH_3{\cdot}H_2O$ (Merck), ethanol (Merck), polyethylene glycol (PEG) 8000 and ultra pure water. Initially, 0.25 M solution of zirconyl nitrate was prepared by dissolving $ZrO(NO_3)_2{\cdot}6H_2O$ in water containing ethanol (18%, v/v). PEG-8000 (2.5%, w/v) was added into the $ZrO(NO_3)_2$ solution. The $NH_3{\cdot}H_2O$ (0.5 M) solution was added drop-wise (3 ml/min) to the $ZrO(NO_3)_2$ solution kept at 80 °C with continuous stirring. The pH of the solution was adjusted to 9. A white, gelatinous precipitate obtained was filtered, washed with ethanol (18%, v/v), dried at 100 °C for 2 h and then calcined at 550 °C for 4 h. Prepared powder was characterized by different techniques to get a complete understanding of its particle size, crystallographic phases and chemical state of zirconium.

2.2. Materials characterization

The Raman spectrum of the prepared powder was obtained using HORIBA Jobin Yvon HR 800 spectrometer with 514.5 nm Ar^+ ion laser.

X-ray photoelectron spectroscopic (XPS) studies were carried out using VG-ESCA Lab MK 200x equipment using Al Kα as the incident X-ray and the data was collected using a hemispherical analyzer kept at 20 eV pass energy.

The XRD patterns were recorded using a Philips (XPERT MPD) X-ray diffractometer employing Cu Kα radiation with 2θ scanning speed of 0.05°/min. TEM studies were carried out in a Philips CM200 ATEM using a LaB_6 filament and an acceleration potential of 200 kV. The ZrO_2 powder were first dispersed in ethanol, sonicated for about 10 min, spread on a 3 mm diameter carbon coated copper grid and finally dried at 40 °C.

2.3. Zeta potential measurements

Nanocrystalline ZrO_2 powder was dispersed in aqueous solution at different pH. The pH of the solution was adjusted by adding dilute solutions of NaOH and HCl. Prior to the measurement of zeta potential, the ZrO_2 particle was suspended in water and sonicated to avoid agglomeration. After sonication, the solution containing the particles was left undisturbed for 24 h to get a stable suspension. Zeta potentials were measured with a Zeta meter (Malvern Instruments, Malvern, UK) by phase analysis light scattering. The light source was He–Ne laser (633 nm) operating at 4.0 mW. The zeta potential values were calculated from the electrophoretic mobility data using Smoluchowsky approximation. The experiment was carried out using a quartz cuvette (universal 'dip' cell) with 10 mm light pathway. These measurements were performed at 25 °C, 40 °C and 70 °C. The effect of widely used dispersant like sodium docecyl sulfate (SDS) on zeta potential of the nanocrystalline ZrO_2 was also studied as a function of pH at 25 °C.

3. Results and discussion

3.1. Micro-structure analysis by TEM and XRD

The bright field TEM micrograph of an agglomerate of the ZrO_2 powder on the carbon film is shown in Fig. 1. The image has been recorded at slight under focus in order to enhance the contrast at the boundaries of the particles. It is observed from the figure that the powder particles are in nanometer size and these nano-particles are faceted indicating their crystalline nature. The sizes of these nano particles are observed to be typically in the range of 10–20 nm. However, for a more accurate estimation of the crystallite size distribution, an image analysis technique was employed on a dark field micrograph shown in Fig. 2. This dark field micrograph was imaged using

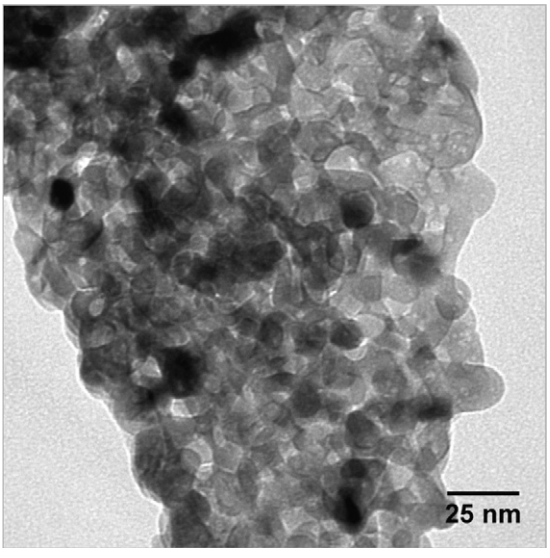

Fig. 1. Bright field TEM micrograph of the ZrO_2 powder showing the nano sized particles.

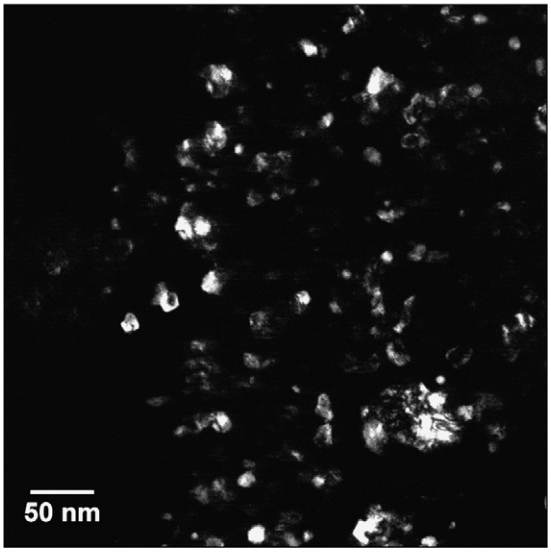

Fig. 2. Dark field TEM micrograph of the powder particles showing nanocrystalline ZrO_2.

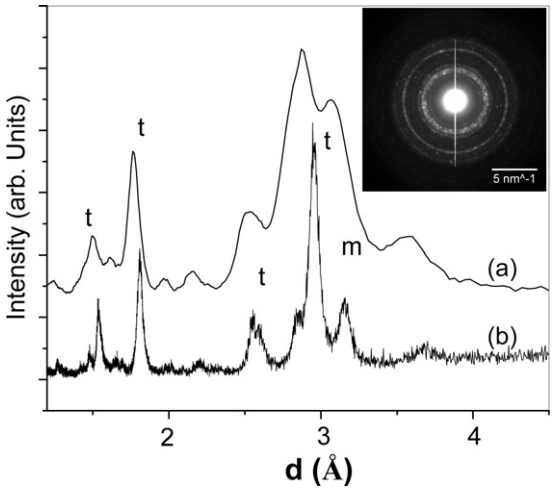

Fig. 4. (a) Electron diffraction pattern evaluated from the image processing technique from SAD pattern shown in the inset, and (b) X-ray diffraction pattern of the nano ZrO_2 powder; peaks corresponding to tetragonal (major) and monoclinic (minor) ZrO_2 phases may be identified from this viewgraph.

the objective aperture around the diffraction spots measuring 2.8–3.1 Å. It is observed from the histogram (Fig. 3) that most of the nano crystals measure 10 nm and some are in the size range of 15–25 nm while a few measure up to 50 nm. This result is consistent with the observation made from the bright field image in Fig. 1 earlier. It is believed that the use of PEG-8000 as steric dispersant controlled the particle size with narrow size distribution. The mechanism of interaction of PEG with precipitated particles is discussed below.

It is known that in the process of formation of nano particles through wet chemistry route, the colloidal stability plays an important role in the development of precipitate morphology [24]. PEG-8000 used in the preparation acts as a steric dispersant. Due to its amphiphilic nature, it can give steric stabilization to control the colloidal interaction potential with its hydrophobic ends adsorbed on the particle surface while the oxyethylene chain stretching into water phase. The precipitated particles are separated from each other due to the surrounding polymer matrix. So PEG adsorbed on the surface of precipitate prevents agglomeration during particle growth and both particle size and distribution would decrease [25].

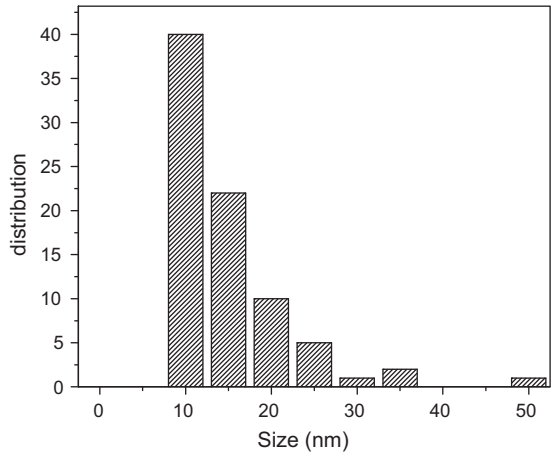

Fig. 3. ZrO_2 crystallite size distribution obtained from analysis of TEM dark field micrograph.

Ethanol as solvent plays important role in ZrO_2 preparation. During powder preparation, if water alone were used, the hydroxide precipitate would have undergone agglomeration due to hydrogen bonds between the particles. This would lead to the formation of hard agglomerates during drying and calcinations. By using the ethanol, hydrogen bond between the adjacent precipitates that are responsible for formation of hard agglomerates were weakened [26] that resulted in the formation of small size fine nanocrystalline ZrO_2.

The X-ray diffraction patterns as well as the electron diffraction pattern recorded from the sample are shown simultaneously in Fig. 4. The electron diffraction pattern has been evaluated by image processing technique from the selected area diffraction (SAD) pattern and is shown in the inset. The reciprocal space unit of the SAD pattern has been converted to actual lattice spacing (d in Å units) after calibration with respect to polycrystalline gold. The background, which contains undefined quantities of contribution from various inelastic scatterings from the sample, has been arbitrarily subtracted in order to compare the peak positions with those of the XRD pattern. Analysis of the XRD pattern reveals two phases of ZrO_2, marked by 't' and 'm' in the figure (Fig. 4) for tetragonal and monoclinic phases, respectively. The broadening of the XRD peaks is attributed to the nanometric sizes of the particles under investigation. The particle sizes (D) were calculated from the Scherrer's formula,

$$D = \frac{0.9\lambda}{\beta \cos\theta}$$

where $\beta^2 = B^2 - b^2$, B and b are the angular half-widths for the sample under investigation and a standard sample, respectively. Analytically pure, crystalline Si powders have been used as the standard sample. Considering λ for Cu Kα as 1.5418 Å, the

calculated average size was observed around 15 nm. Since, XRD measurements reveal the average size of coherent crystalline domains; this result is consistent with our estimation of crystallite size from dark filed TEM imaging shown in Fig. 3, wherein the actual distribution was presented.

Analysis of the electron diffraction pattern reveals that all the diffraction peaks seen in the XRD pattern are present here as well. A small shift of the peak position in the SAD compared to the XRD pattern cannot be understood in terms of inherent inaccuracy in determining '*d*' values from electron diffraction results and calibration. This result also indicates that there is an intimate mixture of the monoclinic and tetragonal ZrO_2 phases even at microscopic scales and not as local clusters of separate monoclinic and tetragonal phases. This observation is consistent with earlier observations by Chraska et al. [27].

3.2. Phase and volume fraction analysis from Raman spectroscopy

TEM and XRD analyses show that the nanocrystalline powder prepared was composed of both tetragonal and monoclinic phases. It is interesting to find the compositions of the phases in the powder. Raman spectroscopy was used to evaluate the quantity of each phase in the powder samples. The corresponding Raman spectrum is shown in Fig. 5. Raman peaks at 148, 269, 317, 462 and 646 cm^{-1} correspond to the tetragonal phase of zirconia, while 180, 192, 379 and 476 cm^{-1} peaks correspond to monoclinic zirconia [28]. The three peaks at 148, 180 and 192 cm^{-1} marked in the figure were taken to estimate the monoclinic phase in the powder.

The fraction of the monoclinic phase (f_m) was estimated using following formula [29]:

$$f_m = \sqrt{0.19 - \frac{0.13}{Xm - 1.01}} - 0.56$$

where

$$Xm = \frac{I(180) + I(192)}{I(148) + I(180) + I(192)}$$

where '*I*' stands for the peak area under respective Raman modes. It worked out to be 35% as monoclinic and 65% as tetragonal phase in the powder.

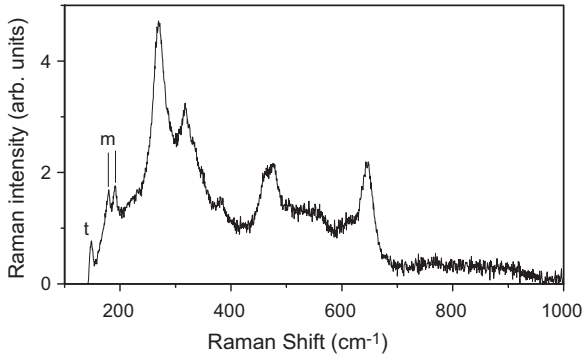

Fig. 5. Raman spectrum of the ZrO_2 powder showing the presence of both tetragonal and monoclinic phases (marked on the spectrum).

It is presumed that nitrate group in $ZrO(NO_3)_2$ has played the vital role in stabilizing the tetragonal phase in the zirconia powder. Precursor obtained from $ZrO(NO_3)_2$ solution exist as $[Zr(OH)_2(OH_2)_2(NO_3)]^+$ chains having one nitrate group covalently bonded to zirconium. The stabilization of tetragonal phase occurred due to the presence of lattice defects or oxygen vacancies created due to the presence of nitrate group covalently bonded to zirconium ion [30,31]. In this context, it can be stated that $ZrOCl_2$ widely used for producing nanocrystalline ZrO_2, is not a preferred material for producing predominant tetragonal phase of nanocrystalline ZrO_2. In case of $ZrOCl_2$, Cl^- ions do not form any complex with zirconium. So creation of oxygen vacancies during thermal annealing in this precursor is unlikely. The oxygen vacancies seem to be responsible for stabilization of tetragonal phase at room temperature. In addition, the presence of nitrate ions retarded the crystallization and delayed the growth of nanocrystalline ZrO_2 powder formed at 550 °C. Metastable tetragonal phase of zirconia is possible to prepare at room temperature without dopants when the particle sizes are below some critical crystallite size around 10–30 nm [7,32]. In the present study, the ZrO_2 particle size distribution (Fig. 3) is in the range of 10–25 nm. This size distribution may be crucial for the tetragonal phase to be dominant in our case. It was observed that the surface free energy favors the stabilization of tetragonal phase below the critical size [33,34]. Thus, it can be concluded that small size of particles are responsible for stabilization of tetragonal phase owing to the lattice distortion caused by NO_3^- ions in the precursor solution.

3.3. Chemical analysis from X-ray photoelectron spectroscopy

X-ray photoelectron spectroscopy measurements were performed to find the chemical composition of the material and the chemical state of Zr in the nanocrystalline ZrO_2 samples. A wide scan of XPS spectrum has been presented in Fig. 6. It is observed that the photoelectron spectrum is

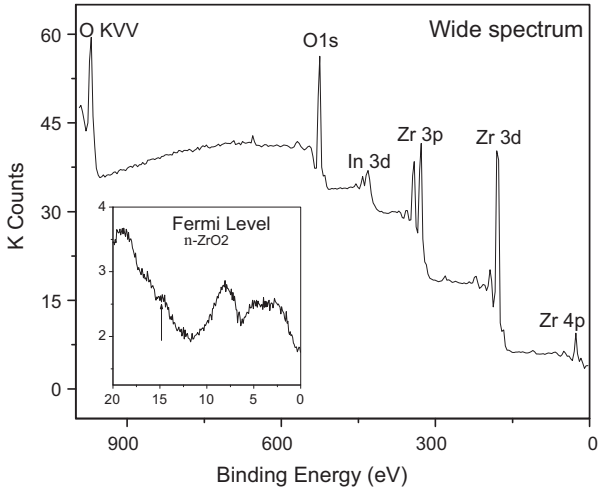

Fig. 6. XPS analysis of ZrO_2 powder on indium foil showing the composition of the powder. The inset of figure shows the near Fermi level spectral features of the powder.

composed of Zr peaks and O peaks. The absence of C indicated that the organic materials used for the preparation was completely burnt out. The indium 4d peak arises from the indium foil used for holding the ZrO_2 powder for XPS experiments. Zr 3d binding energy at around 182 eV indicates the presence of only Zr^{4+} state in these samples. The chemical analysis indicated that the material was not contaminated with any hydroxides or other chemical species.

In the inset of Fig. 6, the near Fermi level spectrum obtained from the powder is also shown. The spectrum is associated with a broad peak from 0 to 7 eV indicating the formation of Zr–O hybridization bonding and non-bonding states [35]. The peak at around 15 eV is Zr 4d occupied states. Though, it is expected that the Zr 4d orbital should be completely unoccupied due to the formation of Zr^{4+} states that gave rise to the Zr4d–O2p conduction band states, the presence of the peak indicates that there is some reduction in Zr oxidation which led to the appearance of the occupied Zr 4d states. The peak around 8 eV is associated with the indium metal which was used for holding the powder for XPS measurements.

3.4. Zeta potential measurements

Effect of temperature and dispersant on charge behavior of zirconia powder was experimentally measured using zeta potential technique. The zeta potential measurements of nanocrystalline ZrO_2 in aqueous suspension was performed at 25, 40 and 70 °C as a function of pH. The detailed results are shown in Fig. 7. The figure shows the pH of zeta potential reversal (pH_{pzc}) decreased from 6.45 to 5.30 with the increase of temperature. The lower pH_{pzc} at higher temperature indicated that the surface hydroxyl groups were more ionized at higher temperature leading to a higher negative surface charge. Thus more protons are required to neutralize the surface charge. This results in shifting the pH_{pzc} to lower pH values [36].

The zeta potential of ZrO_2 in aqueous suspension in presence of 10% sodium docecyl sulfate was determined as a function of pH at 25 °C as shown in Fig. 7d. The figure shows almost a constant high negative zeta potential of ZrO_2 at all pH unlike the systems where SDS was not present. The high negative zeta potential corresponds to the increased stability of the system due to SDS dispersant. SDS is an electrosteric kind of dispersant. In presence of SDS, this behavior of zirconia suspension can be explained by double phase inversion [37], SDS can interact with zirconia both electrostatically (through its sulfate group) and hydrophobically (via its alkane tail-group). Adsorption of SDS molecules on the surface of nanocrystalline zirconia takes place because of coulombic interaction. Beyond a certain SDS concentration, hydrophobic interaction takes place between the alkyl chains of SDS adsorbed on nanocrystalline ZrO_2 in suspension. As a result, the sulfate functional groups are oriented outwards that lead to negative surface charge and negative zeta potential at high SDS concentration. Similar double phase inversion in SDS with $CaCO_3$ was also observed by Cui et al. [37]. So, it is concluded that both functional sulfate group at surface and its hydrophobic chain has influenced the adsorption of SDS on the zirconia/water interface.

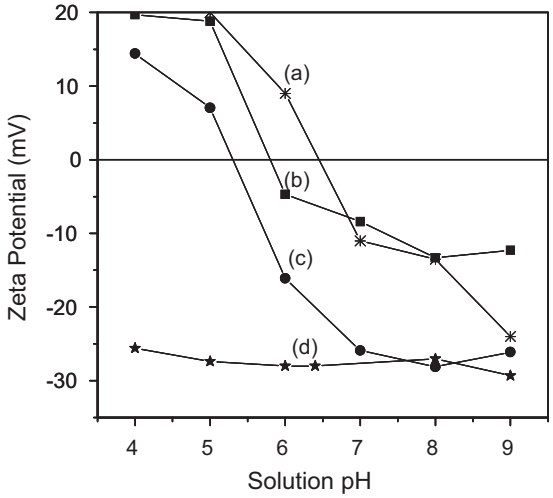

Fig. 7. The zeta potential of the nano ZrO_2 at different temperature, (a) 25 °C, (b) 40 °C and (c) 70 °C, where pH_{pzc} was seen to reduce with increase in the temperature; (d) zeta potential of nano ZrO_2 in the aqueous solution containing SDS.

4. Conclusions

Nanocrystalline zirconia with dominant tetragonal phase has been synthesized by direct precipitation route. The zirconia samples consist of varying sizes but the majority of the nanocrystals are of the order of 10 nm. The charge behavior of the nanocrystalline ZrO_2 in aqueous solution is observed by measuring the zeta potentials. Zeta potential of nanocrystalline ZrO_2 is seen to be negative and stable for a wide range of pH with SDS in solution. These observations may help in deciding appropriate conditions for developing nanocryatelline ZrO_2 coating on steel through hydrothermal process.

Acknowledgements

The authors thank Dr. G. Panneerselvam of IGCAR and Mr. P. Chandramohan of WSCD, BARCF for carrying out XRD and Raman spectroscopy experiments, respectively. They are thankful to Dr. P.A. Hassan and Dr. Gunjan Verma of Chemistry Division, BARC for their guidance for carrying out the zeta potential measurements. They are thankful to Dr. P. Gangopadhaya for carefully going through the manuscript.

References

[1] F. Heshmatpour, R.B. Aghakhanpour, Synthesis and characterization of nanocrystalline zirconia powder by simple sol–gel method with glucose and fructose as organic additives, Powder Technology 205 (2011) 193–200.

[2] M. Atik, S.H. Messaddeq, M.A. Aegerter, Mechanical properties of zirconia-coated 316L Austinitic stainless steel, Journal of Material Science Letters 15 (1996) 1868–1871.

[3] M. Atik, J. Zarzycki, C. R'kha, Protection of ferritic stainless steel against oxidation by zirconia coatings, Journal of Material Science Letters 13 (1994) 266–269.
[4] T.K. Yeh, Y.C. Chien, B.-Y. Wang, C.-H. Tsai, Electrochemical characteristics of zirconium oxide treated Type 304 stainless steels of different surface oxide structures in high temperature water, Corrosion Science 50 (2008) 2327–2337.
[5] L. Borchers, M. Stiesch, F.-W. Bach, J.-C. Buhl, C. Hübsch, T. Kellner, P. Kohorst, M. Jendras, Influence of hydrothermal and mechanical conditions on the strength of zirconia, Acta Biomaterialia 6 (2010) 4547–4552.
[6] T. Chraska, A.H. King, C.C. Berndt, On the size-dependent phase transformation in nanoparticulate zirconia, Materials Science and Engineering A 286 (2000) 169–178.
[7] L. Chen, T. Mashimo, E. Omurzak, H. Okudera, C. Iwamoto, A. Yoshiasa, Pure tetragonal ZrO_2 nanoparticles synthesized by pulsed plasma in liquid, Journal of Physical Chemistry C 115 (2011) 9370.
[8] O. Bernard, A.M. Huntz, M. Andrieux, W. Seiler, V. Ji, S. Poissonnet, Synthesis, structure, microstructure and mechanical characteristics of MOCVD deposited zirconia films, Applied Surface Science 253 (2007) 4626–4640.
[9] G. Rauchs, D. Munz, T. Fett, Calculation of crack tip phase transformation zones with the weight function method, Computational Materials Science 16 (1999) 213–217.
[10] G.N. Heintze, R. Mcpherson, A further study of the fracture toughness of plasma-sprayed zirconia coatings, Surface and Coatings Technology 36 (1988) 125–132.
[11] K. Rodrigo, J. Knudsen, N. Pryds, J. Schou, S. Linderoth, Characterization of yttria-stabilized zirconia thin films grown by pulsed laser deposition (PLD) on various substrates, Applied Surface Science 254 (2007) 1338–1342.
[12] J.R. Vargas Garcia, T. Goto, Thermal barrier coatings produced by chemical vapor deposition, Science and Technology of Advanced Materials 4 (2003) 397–402.
[13] S.T. Aruna, N. Balaji, K.S. Rajam, Phase transformation and wear studies of plasma sprayed yttria stabilized zirconia coatings containing various mol% of yttria, Materials Characterization 62 (2011) 697–705.
[14] I. Espitia-Cabrera, H. Orozco-Hernández, R. Torres-Sánchez, M.E. Contreras-García, P. Bartolo-Pérez, L. Martínez, Synthesis of nanostructured zirconia electrodeposited films on AISI 316L stainless steel and its behaviour in corrosion resistance assessment, Materials Letters 58 (2004) 191–195.
[15] V.K. Balla, P.P. Bandyopadhyay, S. Bose, A. Bandyopadhyay, Compositionally graded yttria-stabilized zirconia coating on stainless steel using laser engineered net shaping (LENS^(TM)), Scripta Materialia 57 (2007) 861–864.
[16] Z.F. Zhou, E. Chalkova, S.N. Lvov, P.H. Chou, Hydrothermal deposition of zirconia coatings on pre-oxidized BWR structural materials, Journal of Nuclear Materials 378 (2008) 229–237.
[17] Z.F. Zhou, E. Chalkova, S.N. Lvov, P. Chou, R. Pathania, Development of a hydrothermal deposition process for applying zirconia coatings on BWR materials for IGSCC mitigation, Corrosion Science 49 (2007) 830–843.
[18] A.J. Kessman, K. Ramji, N.J. Morris, D.R. Cairns, Zirconia sol–gel coatings on alumina–silica refractory material for improved corrosion resistance, Surface and Coatings Technology 204 (2009) 477–483.
[19] T.-K. Yeh, Y.-C. Chien, B.-Y. Wang, C.-H. Tsai, Electrochemical characteristics of zirconium oxide treated Type 304 stainless steels of different surface oxide structures in high temperature water, Corrosion Science 50 (2008) 2327–2337.
[20] P. Jayaweera, S. Hettiarachchi, H. Ocken, Determination of the high temperature zeta potential and pH of zero charge of some transition metal oxides, Colloids and Surfaces A: Physicochemical and Engineering Aspects 85 (1994) 19–27.
[21] Y. Huang, T. Ma, J.-L. Yang, L.-.M. Zhang, J.-T. He, H.-F. LiY, Preparation of spherical ultrafine zirconia powder in microemulsion system and its dispersibility, Ceramics International 30 (2004) 675–681.
[22] Z. Xie, J. Ma, Q. Xu, Y. Huang, Y.-B. Cheng, Effects of dispersants and soluble counter-ions on aqueous dispersibility of nano-sized zirconia powder, Ceramics International 30 (2004) 219–224.
[23] B. Djuricic, S. Pickering, D. McGarry, P. Glaude, P. Tambuyser, K. Schuster, The properties of zirconia powders produced by homogeneous precipitation, Ceramics International 21 (1995) 195–206.
[24] J.L. Look, C.F. Zukoski, Alkoxide-derived titania particles: use of electrolytes to control Size and agglomeration levels, Journal of the American Ceramic Society 75 (1992) 1587–1592.
[25] H.-C. Yao, X.-W. Wang, H. Dong, R.-R. Pei, J.-S. Wang, Z.-J. Li, Synthesis and characteristics of nanocrystalline YSZ powder by polyethylene glycol assisted coprecipitation combined with azeotropic-distillation process and its electrical conductivity, Ceramics International (2011), doi:10.1016/j.ceramint.2011.05.055.
[26] S. Wang, X. Li, Y. Zhai, K. Wang, Preparation of homodispersed nano zirconia, Powder Technology 168 (2006) 53–58.
[27] T. Chraska, A.H. King, C.C. Berndt, On the size-dependent phase transformation in nanoparticulate zirconia, Material Science and Engineering A 286 (2000) 169–178.
[28] P. Barberis, T. Merle-Méjean, P. Quintard, On Raman spectroscopy of zirconium oxide films, Journal of Nuclear Materials 246 (1997) 232–243.
[29] E. Djurado, P. Bouvier, G. Lucazeau, Crystallite size effect on the tetragonal-monoclinic transition of undoped nanocrystalline Zirconia studied by XRD and Raman spectrometry, Journal of Solid State Chemistry 149 (2000) 399–407.
[30] M. Tahmasebpour, A.A. Babaluo, M.K. Razavi Aghjeh, Synthesis of zirconia nanopowders from various zirconium salts via polyacrylamide gel method, Journal of the European Ceramic Society 28 (2008) 773–778.
[31] J. Livage, Sol–gel synthesis of heterogeneous catalysts from aqueous solutions, Catalysis Today 41 (1998) 3–19.
[32] R.C. Garvie, R.H. Hannink, R.T. Pascoe, Ceramic steel, Nature 258 (1975) 703–704.
[33] M. Gateshki, V. Petkov, G. Williams, S.K. Pradhan, Y. Ren, Atomic-scale structure of nanocrystalline ZrO_2 prepared by high-energy ball milling, Physical Review B 71 (2005) 224107–224115.
[34] Z. Qian, J.L. Shi, Characterization of pure and doped ziroconia nanoparticles with infrared transmission spectroscopy, Nanostructured Materials 10 (1998) 235–244.
[35] R.H. French, S.J. Glass, F.S. Ohuchi, Y.-N. Xu, F. Zandiehnadem, W.Y. Ching, Experimental and theoretical studies on the electronic structure and optical properties of three phases of ZrO_2, Physical Review B 49 (1994) 5133–5142.
[36] P. Jayaweera, S. Hettiarachchi, Determination of zeta potential and pH of zero charge of oxides at high temperature, Review of Scientific Instruments 64 (1993) 524–528.
[37] Z.-G. Cui, K.-Z. Shi, Y.-Z. Cui, B.P. Binks, Double phase inversion of emulsions stabilized by a mixture of $CaCO_3$ nanoparticles and sodium dodecyl sulphate, Colloids and Surfaces A: Physicochemical and Engineering Aspects 329 (2008) 67–74.